International Journal of Heat and Mass Transfer 51 (2008) 5958–5974

Contents lists available at ScienceDirect

International Journal of Heat and Mass Transfer

journal homepage: www.elsevier.com/locate/ijhmt

Turbulent conjugate heat and mass transfer from the surface of a binary mixture of ethanol/*iso*-octane in a countercurrent stratified two-phase flow system

R. Banerjee *

Fluid Routing Solutions Inc., 1955 Enterprise Drive, Rochester Hills, MI 48309, United States

ARTICLE INFO

Article history:
Received 15 November 2007
Received in revised form 26 April 2008
Available online 1 July 2008

Keywords:
VOF
Mixture
Evaporation
UNIFAC

ABSTRACT

A numerical study was performed to determine evaporation rate from the surface of a binary mixture of ethanol and *iso*-octane flowing in an inclined 2D channel. The liquid and gas phases are flowing in counter-current direction. VOF multiphase model was used to model stratified two-phase flow. The vapour/liquid equilibrium pressure was calculated using UNIFAC model. Mass transfer contributions from each component evaporating into the carrier gas was calculated and source terms were accordingly implemented in the continuity, momentum, energy and species equations. A parametric study with different inlet and exit conditions was performed.

1. Introduction

Coupled heat and mass transfer for multiphase flow is important in several industrial applications. There is a large body of work where interfacial heat and mass transfer has been investigated for pure substances some of which have been referred here [1–6]. However, analysing momentum, heat and mass transfer for multicomponent fluids are also very important for processes involving mixtures of several components. Due to environmental concerns, there is increased interest in understanding heat and mass transfer of gasoline/alcohol mixtures in the automotive industry.

Early multicomponent evaporation studies were performed for Stefan–Maxwell problem. Taylor [7] formulated a generalized problem for a coupled heat and mass transfer in n-component mixture. Solutions were developed under the assumption of steady one-dimensional transfer. Carty et al. [8] and Mhetar et al. [9] considered evaporation of a binary mixture from the Stefan tube with a stationary and a moving interface, respectively. Several investigators have studied evaporation of multicomponent droplet [10–16] due to its importance in industrial applications like combustion premixing, boiling, condensation, etc.

Numerical and experimental studies have been performed to understand evaporation of multicomponent wall bounded liquid films. Taitel et al. [17] studied evaporation of liquid film in laminar flow. Both Kenig et al. [18] and Palen et al. [19] studied coupled heat and mass transfer from falling liquid film mixtures. Braun et al. [20] studied heat and mass transfer for laminar as well as turbulent falling films in a pipe. They considered the film to be very thin and the liquid phase well mixed. Due to these assumptions, they neglected the convective term in the momentum equation. In a similar treatment, Baumann et al. [21] studied evaporation of a alcohol/hydrocarbon mixture and took into consideration the phase equilibrium of binary liquids and multicomponent thermodynamics. Gerendas et al. [22] performed experimental and numerical study to investigate the evaporation of water and ethanol mixture on liquid wall films. They took into account the effect of wavy liquid surface due to interfacial shear stress on momentum, energy and species equation. In their study, they considered only the gas phase flow and neglected the liquid phase flow. When the film thickness is very small, such assumptions are valid [23]. However, for bulk flows, where the liquid film thickness is significant, both liquid and gas phase flows should be solved simultaneously.

When considering multiphase flow, different interface tracking methods have been proposed like VOF [24], level set [25], front tracking or immersed boundary [26] methods. The VOF method was previously used to study heat and mass transfer in droplets [27,28], bubbles [29] and film boiling [30,31]. However, all the above investigations were done on pure fluids. In the present study, a heat and mass transfer algorithm for liquid mixtures was developed. This algorithm was then used in conjunction with VOF multiphase model to study heat and mass transfer under stratified flow condition. As mentioned before, there is a lot of interest in understanding heat and mass transfer of gasoline/alcohol mixture in the automotive industry. However, gasoline is a very complex mixture composed of hundreds of different components. Therefore, in this study, *iso*-octane has been used as its surrogate

* Tel.: +1 248 844 1187; fax: +1 248 853 5153.
E-mail address: raja.banerjee@fluidrouting.com

0017-9310/$ - see front matter © 2008 Elsevier Ltd. All rights reserved.
doi:10.1016/j.ijheatmasstransfer.2008.04.057

Nomenclature

$\boldsymbol{A}$	surface area normal (m^2)
C_p	specific heat (J/kg K)
D, D_{ij}	binary diffusivity (m^2/s)
E	energy (J/kg)
$\boldsymbol{g}$	acceleration due to gravity (m/s^2)
h	enthalpy (J/kg)
h_{fg}	latent heat of vapourization (J/kg)
h_w	wall heat transfer coefficient (W/m^2 K)
$\boldsymbol{J}$	species flux (kg/m^2 s)
k	thermal conductivity (W/m K)
M	molecular weight (kg/kmol)
$\dot{m}$	mass transfer rate (kg/s)
m_i'''	mass transfer/volume (kg/m^3 s)
p, P	pressure (Pa)
R	universal gas constant (J/kg K)
S	source term (kg/m^3)
S_e	source term, energy equation (W/m^3)
S_m	source term, momentum equation (N/m^3)
$S_{\alpha q}$	source term, VOF equation (kg/m^3)
T	temperature (K)
t	time (s)
$\boldsymbol{u}$, u	velocity (m/s)
V_{cell}	volume of computational cell (m^3)
X	liquid phase mole fraction
x	gas phase mole fraction
Y	liquid phase mass fraction
y	gas phase mass fraction
Z	compressibility factor

Greek symbols

α	volume fraction
γ	activation coefficient
η	evaporation efficiency
μ	viscosity (Pa s)
ρ	density (kg/m^3)

Subscripts

i	inlet
e	exit
q	qth fluid
eff	effective
g	gas phase
l	liquid phase
v	vapour
C	critical

Superscripts

i, j	i or jth species
m	mixture

fluid. All computations have been done using commercially available CFD code FLUENT 6.3 [32].

2. Mathematical formulation

In this investigation numerical analysis has been performed to study evaporation from the surface of a binary mixture of ethanol and *iso*-octane. As shown in Fig. 1, liquid is flowing over an inclined 2D channel with the gas phase flowing in the opposite direction due to higher backpressure. The vertical plane where the liquid phase enters the channel is defined as the channel inlet and the vertical plane where the liquid phase exits the channel is defined as channel exit. The bottom wall is maintained at a constant temperature of T_w. At the top wall convective heat transfer is taking place with the coefficient of heat transfer being h_w and free stream temperature is T_∞. The liquid inlet velocity and temperature is u_i and T_i, respectively. The exit backpressure and temperature is P_e and T_e, respectively.

Due to their volatile nature, liquid ethanol and *iso*-octane evaporate into the adjacent air stream. Therefore, the gas phase is a tertiary mixture of ethanol, *iso*-octane and air. The mass fraction of all the species in the gas and liquid phase is tracked. Heat transfer due to evaporative cooling is also included in addition to sensible heat transfer taking place due to non-isothermal conditions in the flow domain.

2.1. Governing equations

2.1.1. Multiphase model

Counter-current stratified flow of liquid and gas phase in a channel can be solved using VOF multiphase model. The VOF model is a fixed grid technique, which can be used to model two or more immiscible fluids. This model solves a single set of momentum equations shared by the fluids, and the volume fraction of each fluid in the computational cell is tracked throughout the domain. Interface tracking is accomplished by the solution of a transport equation for the volume fraction of one of the phases. This equation has the following form:

$$\frac{1}{\rho_q}\left[\frac{\partial}{\partial t}(\alpha_q\rho_q) + \nabla\cdot(\alpha_q\rho_q\boldsymbol{u}_q) = S_{\alpha q}\right] \tag{1}$$

The volume fraction α_q can have the following values:

$\alpha_q = 1$ if the cell is completely filled with qth fluid.
$\alpha_q = 0$ if the cell is empty of qth fluid.
$0 < \alpha_q < 1$ if the cell is partially filled with qth fluid.

The volume fraction for the primary phase is not solved as it can be computed based on the following constraint

$$\sum_{q=1}^{n}\alpha_q = 1 \tag{2}$$

The gas phase was taken as the primary phase in this study. As there are only two phases in the flow domain, $n = 2$. Transport properties that appear in the conservation equations are determined from the volume fraction of each phase. For example, density can be expressed as,

$$\rho = \sum \alpha_q\rho_q \tag{3}$$

A control-volume formulation requires that convection and diffusion fluxes through the control-volume faces be computed and balanced with the source terms within the control-volume itself. The geometric reconstruction algorithm was used to determine the face fluxes for the VOF model. The geometric reconstruction scheme represents the interface between fluids using a piecewise-linear approach. It assumes that the interface between the two-fluids has a linear slope within each cell, and uses this property to calculate the advection of fluid through the cell faces using a geometric reconstruction scheme. The other conservation equations are of the form:

Momentum equation

A single momentum equation is solved throughout the flow domain and the resulting velocity field is shared among the phases.

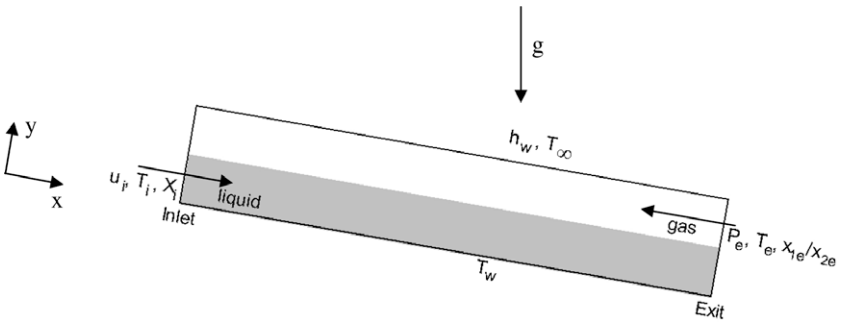

Fig. 1. Schematic of flow domain.

The momentum equation is dependent on the volume fraction of all phases through the transport properties of ρ and μ:

$$\frac{\partial}{\partial t}(\rho \boldsymbol{u}) + \nabla \cdot (\rho \boldsymbol{u}\boldsymbol{u}) = -\nabla p + \nabla \cdot [\mu_{\text{eff}}(\nabla \boldsymbol{u})] + \rho \boldsymbol{g} + S_{\text{m}} \tag{4}$$

Energy equation

The energy equation is also shared by between the two phases

$$\frac{\partial}{\partial t}(\rho E) + \nabla \cdot [\boldsymbol{u}(\rho E + p)] = \nabla \cdot \left(k_{\text{eff}} \nabla T - \sum_j h^j \boldsymbol{J}^j \right) + S_{\text{e}} \tag{5}$$

Energy, E and temperature, T are mass-averaged variables as shown below,

$$E = \frac{\sum_{q=1}^{n} \alpha_q \rho_q E_q}{\sum_{q=1}^{n} \alpha_q \rho_q} \tag{6}$$

Species equation

Phase specific species equation is solved with VOF model and is expressed as,

$$\frac{\partial}{\partial t}(\rho_q \alpha_q y_q^i) + \nabla \cdot (\rho_q \alpha_q \boldsymbol{u} y_q^i) = -\nabla \cdot (\alpha_q \boldsymbol{J}_q^i) + S^i \tag{7}$$

The diffusion flux term that appear is Eqs. (5) and (7) is given as

$$\boldsymbol{J}^i = -\rho D_{\text{eff}}^i \nabla y^i \tag{8}$$

As the gas phase is a tertiary mixture of ethanol, *iso*-octane and air, a set of two species equations to track ethanol and *iso*-octane vapour are solved in the gas phase. One species equation to track liquid ethanol is solved in the liquid phase.

Turbulence equation

Several turbulence models are available in FLUENT. A previous study [33] has shown that RNG-k–ε model is best suited for stratified two-phase flow. Hence, RNG-k–ε model was used for all calculations in this study.

2.2. Interface conditions

Due to volatile nature of liquid phase mixture, mass transfer due to evaporation takes place from the liquid phase to the gas phase. Different methods have been used to determine the interfacial mass flux term. Wohak et al. [27] calculated it from the heat flux based on the temperature gradient of the previous time step; Harvie et al. [28] used a model based on a kinetic theory treatment and Welch et al. [30,31] used the relative velocity of the gas or liquid phase adjacent to the interface. In this study, mass flux term was obtained directly from the normal component of species gradient at the interface. Evaporation rate per unit volume can thus be expressed as,

$$m_i''' = \frac{\dot{m}^i}{V_{\text{cell}}} = -\rho_{\text{g}} D_{\text{eff}}^i \nabla y^i \cdot \frac{\boldsymbol{A}}{V_{\text{cell}}} \tag{9}$$

where, the liquid/gas interface surface area normal is given by,

$$\boldsymbol{A} = V_{\text{cell}} \nabla \alpha_{\text{g}} \tag{10}$$

The surface area normal vector is pointing towards the gas phase. Combining Eqs. (9) and (10), the evaporation rate can be expressed as,

$$m_i''' = -\rho_{\text{g}} D_{\text{eff}}^i \nabla y^i \cdot \nabla \alpha_{\text{g}} \tag{11}$$

A more robust mass transfer formulation is

$$m_i''' = -2\alpha_{\text{l}} \rho_{\text{g}} D_{\text{eff}}^i \nabla y^i \cdot \nabla \alpha_{\text{g}} \tag{12}$$

where, the term $2\alpha_{\text{l}}$ is being used to moderate mass transfer, similar to using an under-relaxation factor. As liquid/gas interface is defined when volume fraction is equal to 0.5, evaporation is occurring when liquid volume fraction is less than 0.5. Hence, the value of the term $2\alpha_{\text{l}}$ is always less than 1. Therefore, a computational cell where liquid volume fraction is zero, mass transfer rate is also zero even though the dot product of mass fraction gradient and volume fraction gradient may be a non-zero term. Mass transfer term as expressed in Eq. (12) was used in this study.

Due to evaporation from the surface of the liquid phase, source terms appear in the governing equations.

VOF equation

For the liquid phase the source term is

$$S_{\alpha \text{l}} = -\sum_{i=1}^{N} m_i''' \tag{13}$$

and for gas phase the source term is

$$S_{\alpha \text{g}} = \sum_{i=1}^{N} m_i'''$$

As interfacial mass transfer is being calculated for ethanol and *iso*-octane, $N = 2$ in this study.

Momentum equation

Due to evaporation, momentum is lost in the liquid phase and it is gained in the gas phase. Therefore, a volume fraction averaged momentum equation source term can be expressed as,

$$S_{\text{m}} = (1 - 2\alpha_{\text{l}}) \sum_{i=1}^{N} m_i''' \boldsymbol{u} \tag{14}$$

A more detailed derivation of Eq. (14) is given in Ref. [37].

Energy equation

The source for the energy equation is

$$S_{\text{e}} = -\rho \sum_{i=1}^{N} \frac{m_i'''}{\rho_{\text{l}}} h_{\text{fg}}^i \tag{15}$$

Species equation

As two species equations are solved in the gas phase, evaporation rate of ethanol is applied as the source term in the species

equation tracking ethanol. Similarly, evaporation rate of *iso*-octane is applied to the *iso*-octane species equation. Therefore, source term for the gas phase species equations is expressed as,

$$S^i = m_i''' \tag{16}$$

Only ethanol is tracked in the liquid phase. Hence, the relative evaporation rate of ethanol with respect to *iso*-octane is applied as the source term for the liquid phase species equation. It is expressed as,

$$S^i = m'''_{C_2H_5OH} - m'''_{C_8H_{18}} \tag{17}$$

Interface mole/mass fraction

The binary mixture of ethanol and *iso*-octane is a non-ideal mixture due to high polarity of ethanol molecule. Therefore, vapour pressure of the mixture is very strongly dependent on the composition of the liquid. Liquid/gas interface vapour mole fraction is given by,

$$x^i = \eta \frac{\gamma^i X^i P^i_{vap}}{P} \tag{18}$$

where γ^i is the activation coefficient of the ith species. The activation coefficient has been calculated using UNIFAC method as described in Ref. [34]. Fig. 2 shows the profile of ethanol vapour mass fraction and total vapour pressure for different liquid composition. Under equilibrium conditions, the vapour at the interface will be saturated. However, under a dynamic system, such as this study where the residence time is low, equilibrium conditions are difficult to reach. Therefore, it is assumed that vapour at the interface does not reach saturation and hence, an efficiency term, η has been introduced. As good experimental results are lacking for the present study, η has been assumed to be 0.25. Harvie et al. [35] have previously used accommodation coefficient to account for interfacial resistance to heat and mass transfer.

The interface mass fraction is calculated from,

$$y^i = \frac{x^i M^i}{\sum_{i=1}^{N} x^i M^i} \tag{19}$$

3. Solution method

FLUENT uses a control-volume-based technique to convert the governing equations into algebraic equations that can be solved numerically. Second order discretization scheme was used to discretize all the transport equations. As body force due to gravity is present in all the cases, body weighted pressure discretization scheme was used. SIMPLEC algorithm was used for pressure–velocity coupling.

As shown in Eqs. (9)–(12), evaporation rate of ith species is governed by the gradient of mass fraction of the ith species at the liquid/gas interface. However, unlike momentum and energy equations, species equation is not shared by all the phases and it is solved for individual phases. Species equation for ethanol and *iso*-octane vapour is solved only in the gas phase and is not solved in the liquid phase. Similarly, species equation for liquid ethanol is solved only in the liquid phase. This leads to discontinuity at the liquid/gas interface in the species equation resulting in non-physical values for vapour mass fraction gradient at the interface. Therefore, interfacial mass transfer values as calculated from Eq. (12) will not be correct. To overcome this problem, one dummy variable, corresponding to each of the species being solved in the gas phase, was used. These variables are available in the whole flow domain and hence shared by both phases. These variables were assigned the interfacial mass fraction using Eq. (19) for any computational cell which is either partially or completely filled with liquid. In the rest of the flow domain, the magnitude of the dummy variables was equal to the vapour mass fractions. Therefore, evaporation rate was calculated using gradient of these dummy variables at the liquid/gas interface.

The use of such user defined variables has been previously used by the author [36,37] in studying evaporation of pure fluids. As these variables are solvable in the whole flow domain, in the first study [36], saturated vapour mass fraction was assigned in the liquid phase using the concept of "internal" boundary condition [38]. To determine mass transfer in the gas phase, a transport equation of this variable was solved in-lieu of the species equation. This algorithm was systematically evaluated through a series of test cases and mass fraction in the gas phase was compared against

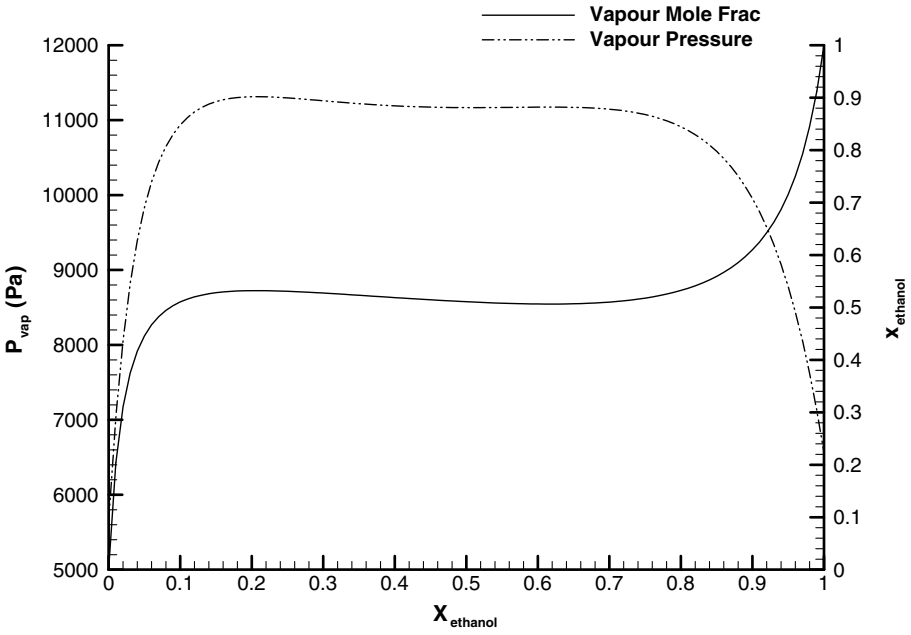

Fig. 2. Change in vapour liquid equilibrium with mixture composition.

Table 1
Important data

Properties	Data		
	Ethanol	*iso*-Octane	Air
T_C (K)	513.92	543.90	
P_C (bar)	61.48	25.7	
ω	0.649	0.304	
Dipole (debye)	1.7	0.0	
Molecular weight	46.069	114.231	28.8
k vapour (W/m K)	0.0154	0.0117	0.0242
k liquid (W/m K)	0.182	0.0995	
μ vapour (Pa s)	8.5753×10^{-5}	0.593×10^{-5}	1.7894×10^{-5}
μ liquid (Pa s)	0.001233	0.000455	
C_p vapour (J/kg K)	1006	1006	1006
C_p liquid (J/kg K)	2470	2037	
ρ liquid (kg/m^3)	813	695.5	

analytical solutions. However, sensible and latent heat transfer was neglected in this study. In the second study [37], these restrictions were removed with the actual calculation of interfacial mass transfer from the gradient of the user defined variable at the liquid/gas interface. The present study is an extension of the last study by taking into account heat and mass transfer of non-ideal liquid mixtures.

The gas phase is a tertiary mixture of ethanol, *iso*-octane and air and the liquid phase is a binary mixture of ethanol and *iso*-octane. The thermophysical properties of all the species in the liquid and gas phases are given in Table 1. Various models have been used to determine VLE and mixture properties and have been referred from Poling et al. [34]. Wagner method for ethanol and Antoine method for *iso*-octane were used to calculate the vapour pressure and heat of vapourization. For the gas phase, molecular diffusivity of each pair of species were calculated using Fuller method. This was then used to calculate effective diffusivity using the mixture formulation as explained in the Appendix. Gas phase viscosity and thermal conductivity were calculated using mixture theory proposed by Wilke and Mason & Saxena, respectively. The gas phase specific heat was assumed to be independent of composition and therefore taken as a constant in the whole flow domain. Liquid

Table 2
Summary of grid independence study

Grid	Bottom wall heat flux (W/m)	Evaporation rate (kg/m s)10^{-3}	Latent heat of evaporation (W/s)
3500	23,165	2.596	1310
8600	22,962	2.810	1419
13,000	22,902	2.838	1433

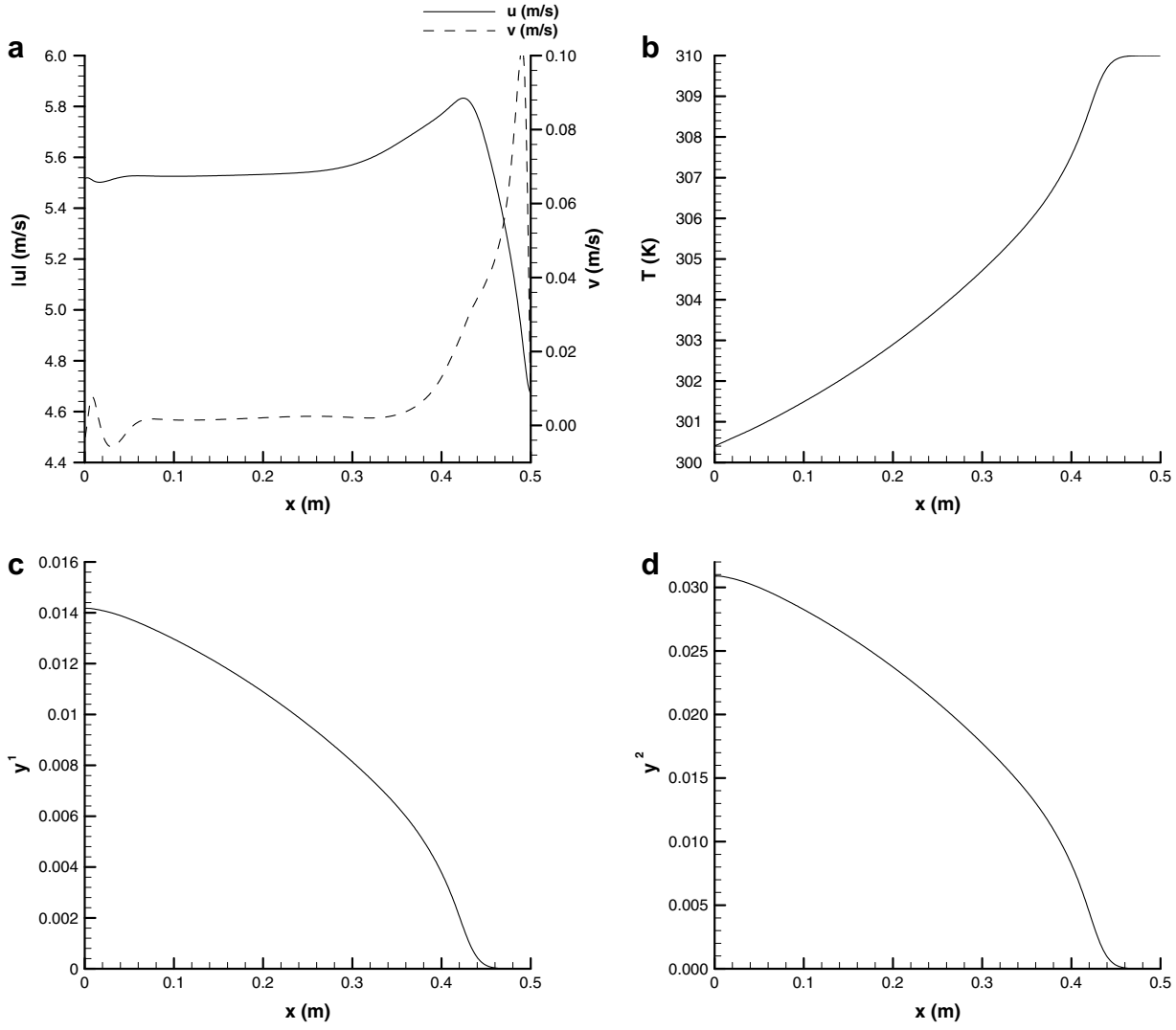

Fig. 3. Gas phase: (a) x- and y-velocity profiles, (b) temperature, (c) ethanol mass fraction and (d) *iso*-octane mass fraction at $y = 20$ mm.

phase density was calculated from the mole fraction of individual components. Grunberg and Nissan method was used to calculate liquid mixture viscosity and thermal conductivity was calculated from Power Law method. FLUENT's mass based mixture model was used to calculate liquid specific heat. The Appendix describes in detail the calculation procedure of the transport properties in both the phases.

4. Results and discussion

The schematic of the problem setup is shown in Fig. 1. The geometry and grid was created in GAMBIT, the pre-processor of FLUENT. The geometry consists of a 2D channel with 500 mm in length and 25 mm high. The channel is inclined at an angle of 5° for gravity-assisted flow. Liquid is introduced into the channel from the bottom left corner and height of the liquid phase at the entrance in 12.5 mm. The reverse flowing air/vapour mixture is introduced from the right hand side of the channel due to higher backpressure. The bottom left corner of the channel is the origin of the x- and y-coordinate system.

Initially, a base case was modelled with liquid phase inlet condition: $u_i = 2$ m/s, $T_i = 295$ K, $X_{1i} = 0.2$, exit condition: $P_e = 50$ Pa (gauge), $T_e = 310$ K, $x_{1e}/x_{2e} = 0/0$, top wall condition: $h_w = 1.5$ W/m^2 K, $T_\infty = 300$ K and bottom wall condition: $T_w = 320$ K. By systematically changing some of the boundary conditions, variations in some of the key results were recorded. The following are the set of simulations that were performed:

- Set 1: Exit temperature, T_e: 310, 320, 330 and 340 K.
- Set 2: Exit pressure, P_e: 30, 50, 70 and 90 Pa (gauge).
- Set 3: Exit gas phase composition, x_{1e}/x_{2e}: 0/0, 0/10, 10/0 and 10/10.
- Set 4: Inlet liquid temperature, T_i: 295, 310, 325 and 340 K.
- Set 5: Inlet liquid composition, X_{1i}: 0%, 20%, 50%, 80% and 100%.

In all the simulation sets, all the parameters are maintained at the base condition except for the parameter that is varied.

A uniform grid was created to simulate flow in the fluid domain. The base case was solved with various grid configurations to obtain a grid independent solution. Initially, a grid with 222 elements in the longitudinal direction and 16 elements in the transverse direction was used. This grid was further refined such that grids with 333×26 and 417×32 were created. Grid independence can be checked using various parameters. In this study wall flux due to non-adiabatic wall conditions and bulk quantities due interfacial heat and mass transfer are important. Therefore, as shown in Table 2, total heat flux from the bottom wall, evaporation rate and total latent heat of vapourization has been used to determine grid independence. It can be seen that all the three parameters change by less that 1% when the grid was refined from 333×26 to 417×32. Therefore, it was assumed that grid independence was achieved and grid with 417×32 was used to simulate the rest of the cases. An unsteady simulation was performed with a time step size of 5×10^{-4} s. The simulations were performed till steady flow was achieved. Steady flow was considered achieved when the total

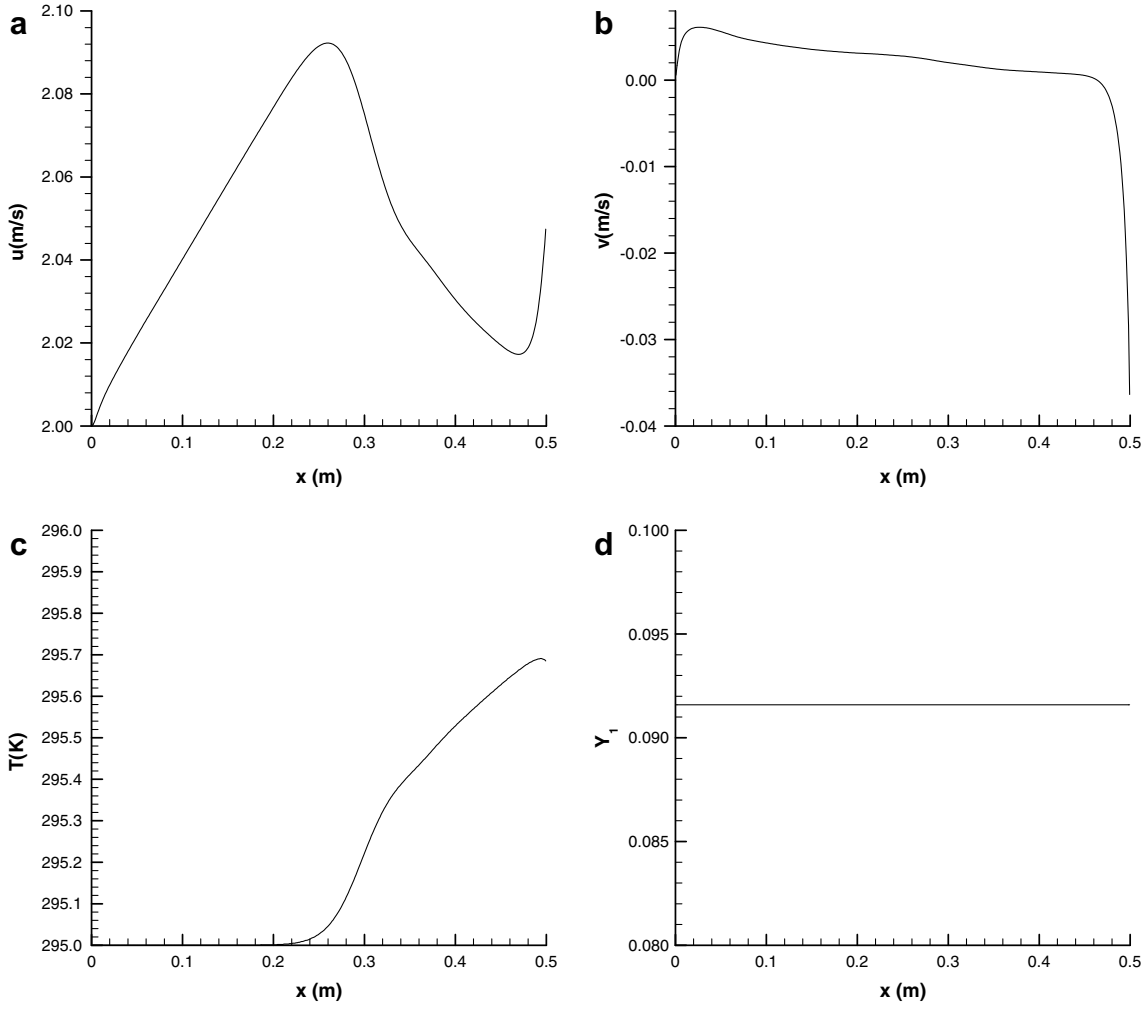

Fig. 4. Liquid phase: (a) x-velocity profile, (b) y-velocity profile, (c) temperature and (d) ethanol mass fraction at $y = 5$ mm.

evaporation rate did not change with time. For the base case, steady flow was reached after about 15 s of flow time.

4.1. Base case

In a counter-current system, liquid phase close to the channel exit is fully developed. However, the gas phase is still developing. Similarly, close to the channel inlet, the liquid phase is still developing but the gas phase is fully developed. Due to this fact, shearing interaction between the two phases is large close to the inlet and exit of the channel. Fig. 3 shows the gas phase velocity, temperature and mass fractions of ethanol and *iso*-octane vapour at $y = 20$ mm. As in any typical wall bounded flow, the longitudinal and transverse velocity component initially increases as the air/vapour mixture enters the channel from the right hand side. However, due to interfacial shearing interaction originating from the counter flowing liquid phase and also momentum diffusion due to the top wall, velocity magnitude starts decreasing after a certain

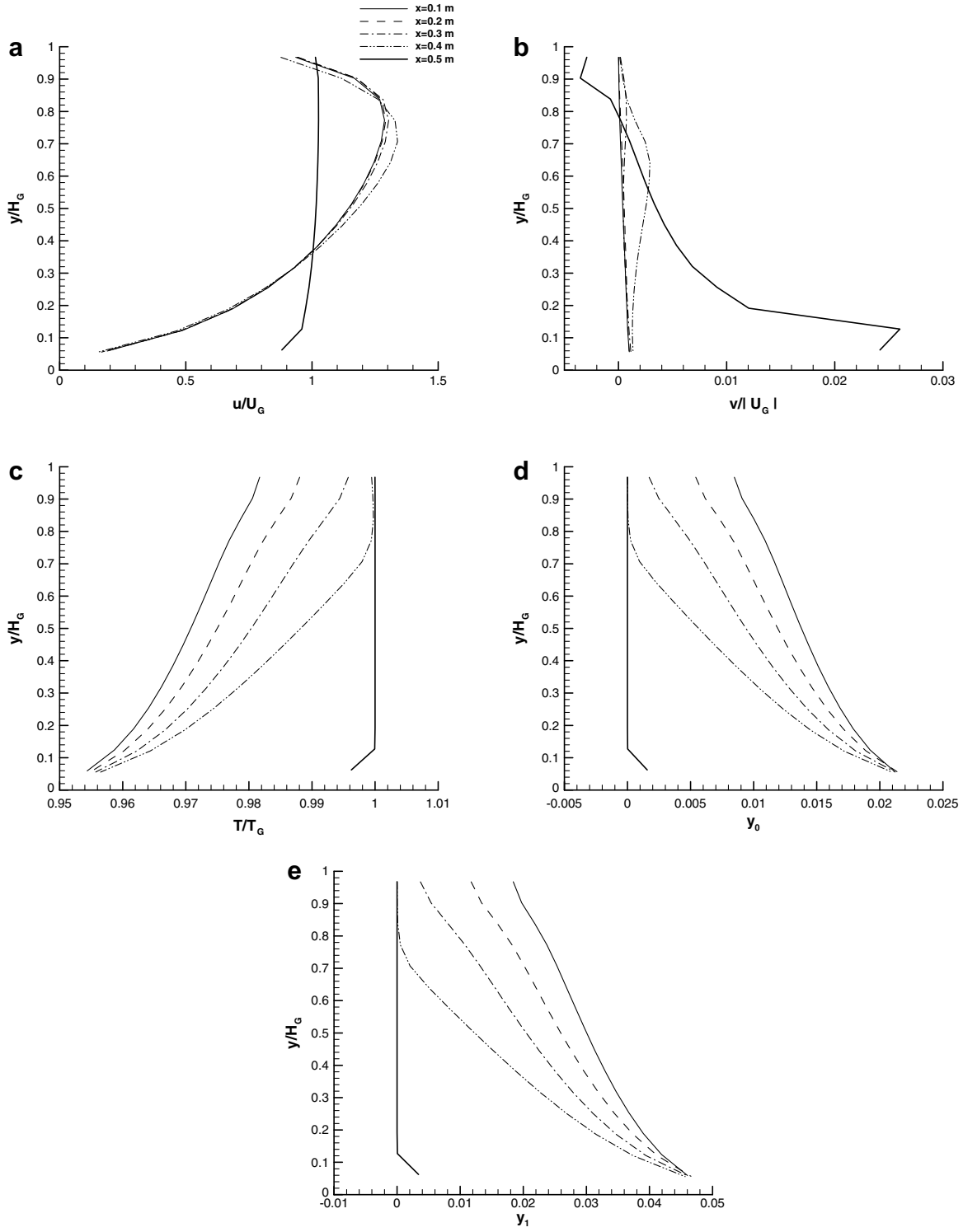

Fig. 5. Gas phase: (a) *x*-velocity profile, (b) *y*-velocity profile, (c) temperature, (d) ethanol mass fraction and (e) *iso*-octane mass fraction at $x = 0.1$, 0.2, 0.3, 0.4 and 0.5 m.

distance from the exit. Finally, it reaches a steady value, which it maintains for the rest of the channel. Gas phase temperature and vapour mass fractions of ethanol and *iso*-octane initially maintain their exit condition close to the channel exit. The temperature starts decreasing and vapour mass fractions start increasing once the thermal and species layers reaches $y = 20$ mm. It must be noted that mass transfer from the liquid phase should accelerate the gas phase. However, in this case, at $y = 20$ mm, the momentum transfer due to interfacial shearing interaction and pressure of the top wall predominates.

Fig. 4 shows the liquid phase velocity, temperature and ethanol mass fraction profiles at $y = 5$ mm. As seen in the gas phase the longitudinal velocity initially increases. After a certain distance from the inlet, the magnitude then decreases. This is because, beyond this distance horizontal plane of $y = 5$ mm is within the boundary layer due to the bottom wall. Unlike in the gas phase, the increase in the longitudinal velocity component magnitude is more prolonged. This is because liquid density is almost three orders higher than gas phase density, which in turn results in lower effective kinematic viscosity in the liquid phase. Hence, momentum diffusion in the liquid phase is slower. The vertical velocity component steadily decreases along the length of the channel. As the bottom wall temperature is 320 K, there is heat transfer from the wall to the liquid volume. Temperature starts increasing after a certain distance downstream from the liquid inlet. This distance is approximately same when longitudinal velocity component starts decreasing; thereby indicating that at this distance momentum and thermal diffusion due to wall effects starts being significant. However, as there is no change in liquid ethanol mass fraction as $y = 5$ mm, it can be concluded that interfacial effects are not significant at this horizontal plane.

Figs. 5 and 6 show the two velocity components, temperature and species mass fractions at five vertical planes in the gas and liquid phases, respectively. In each phase, the velocity components, temperature and height are normalized by their respective inlet area-averaged velocity, temperature and height. At $x = 0.5$ m, air/vapour mixture is entering the channel and therefore the x-velocity component is almost uniform. Due to developing nature of flow at this location, the y-velocity component changes from positive value close to the liquid/gas interface to negative value close to the top wall. As the liquid is flowing in the opposite direction, y-velocity magnitude has larger values close to the interface. Away from the channel exit, as the flow becomes more developed, both the velocity components attain a steady magnitude. As the gas phase is entering the channel at a higher temperature than the liquid phase and also due to latent heat transfer, gas phase temperature decreases away from the wall and is lowest at the liquid/gas interface in all the vertical planes other than at $x = 0.5$ m. As the air/vapour mixture travels upstream in the channel, the temperature magnitude decreases at successive vertical planes due to heat transfer taking place at the liquid/gas interface and at the top wall. Mass fraction of ethanol and *iso*-octane vapour mass fraction

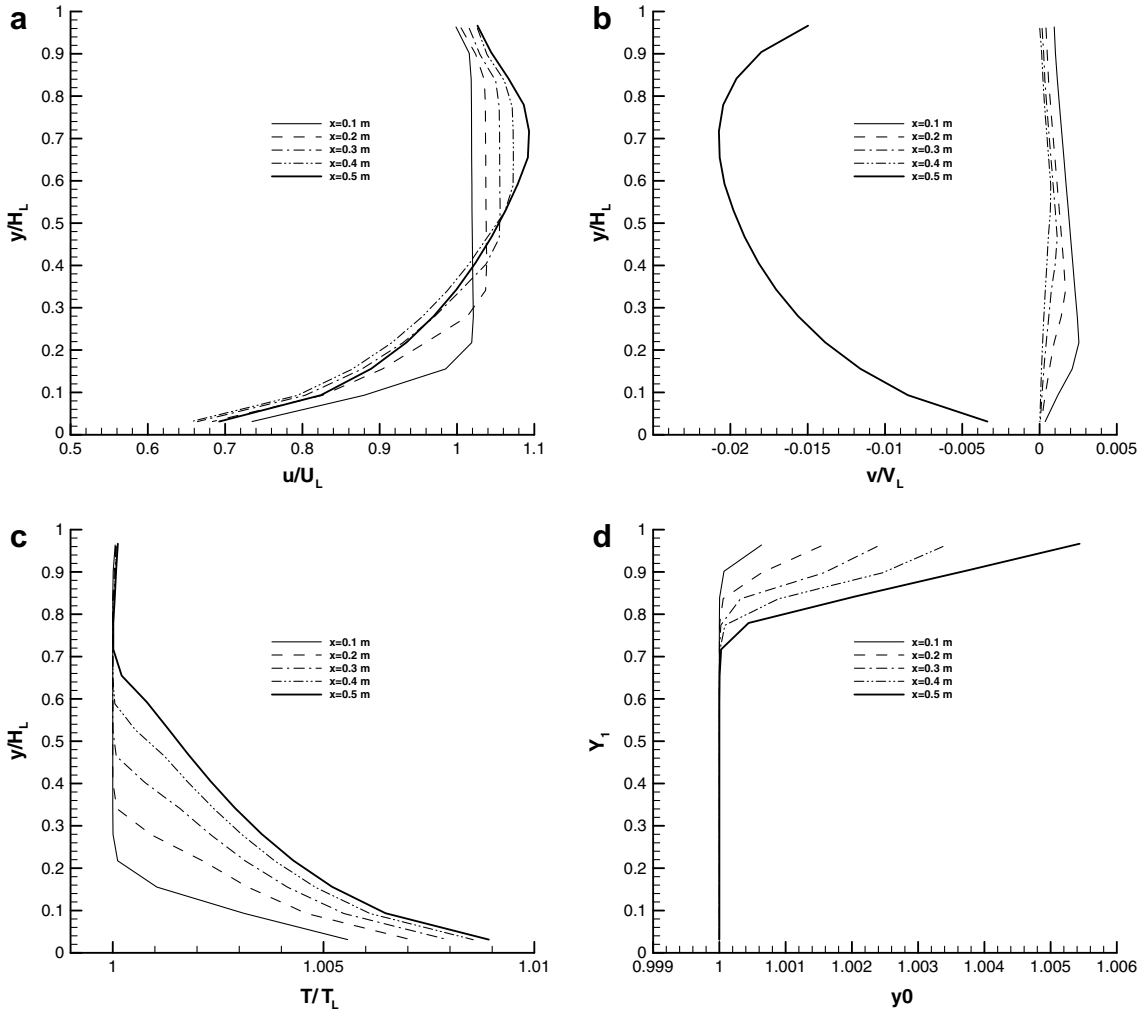

Fig. 6. Liquid phase: (a) x-velocity profile, (b) y-velocity profile, (c) temperature and (d) ethanol mass fraction at $x = 0.1$, 0.2, 0.3, 0.4 and 0.5 m.

increases as the gas phase travels upstream in the channel due to interfacial mass transfer. In the liquid phase, *x*-velocity component is seen developing from the inlet to the exit of the channel and the slope is negative near the liquid/gas interface because the gas phase is flowing in the opposite direction. As the liquid and gas phases are flowing in a counter-current system, the *y*-velocity component changes from being positive close to the inlet to being negative at the channel exit. Liquid temperature increases away from the liquid/gas interface and is highest close to wall due to sensible heat transfer from the wall. This rise in temperature is more apparent as the liquid flows downstream. However, as can be seen from Fig. 6, the magnitude of temperature rise is not large. Also, as the temperature close to the interface is almost same as the inlet temperature, interfacial latent heat transfer is small compared to sensible heat transfer from the bottom wall. The mass fraction of liquid ethanol is increasing near the interface as the liquid flows downstream indicating that the evaporation rate of *iso*-octane is higher than ethanol. This is because, even though vapour pressure of ethanol for a given temperature is higher than *iso*-octane, molecular weight of *iso*-octane is higher than ethanol, resulting in higher evaporation rate is terms of mass per unit time.

Fig. 7 shows flow parameters at liquid/gas interface. The interface is defined where the volume fraction of liquid is 0.5. There is an increase in the *x*-velocity magnitude along the length of the channel. This can be attributed to the fact the channel is inclined at 5° and the increase is due to acceleration due to gravity. Due to interfacial mass transfer, there is a positive flow from the liquid phase to the gas phase, which is shown in the positive value of *y*-velocity component at the interface. The interfacial temperature remains close to the liquid inlet temperature of 295 K along most of the length of the channel. It must be noted here that even though evaporation rate of *iso*-octane is higher that ethanol, latent heat transfer due to evaporating ethanol is marginally higher than *iso*-octane. This is because, latent heat of vapourization of ethanol is much higher than *iso*-octane. Fig. 8 shows the thermal profiles of top and bottom walls. As energy is being lost from the fluid domain across the top wall, heat flux has a negative sign. As expected, heat flux magnitude is highest near the channel exit and it decreases as the air/vapour mixture flows upstream. Similarly, the top wall temperature reduces from the exit to the inlet of the channel. At the bottom wall, heat transfer is taking place from the wall to the liquid phase and therefore it has a positive sign. Its magnitude is decreasing along the length of the channel.

4.2. Parametric study

As explained before, a parametric study was done by varying the inlet and exit boundary conditions. The effect of these parameters on interfacial flow characteristics were recorded at two locations: $x = 0.15$ and 0.35 m. Liquid/gas interface was defined where the liquid volume fraction was equal to 0.5. Fig. 9 shows the results from Set 1, where the exit temperature was varied. For all the cases

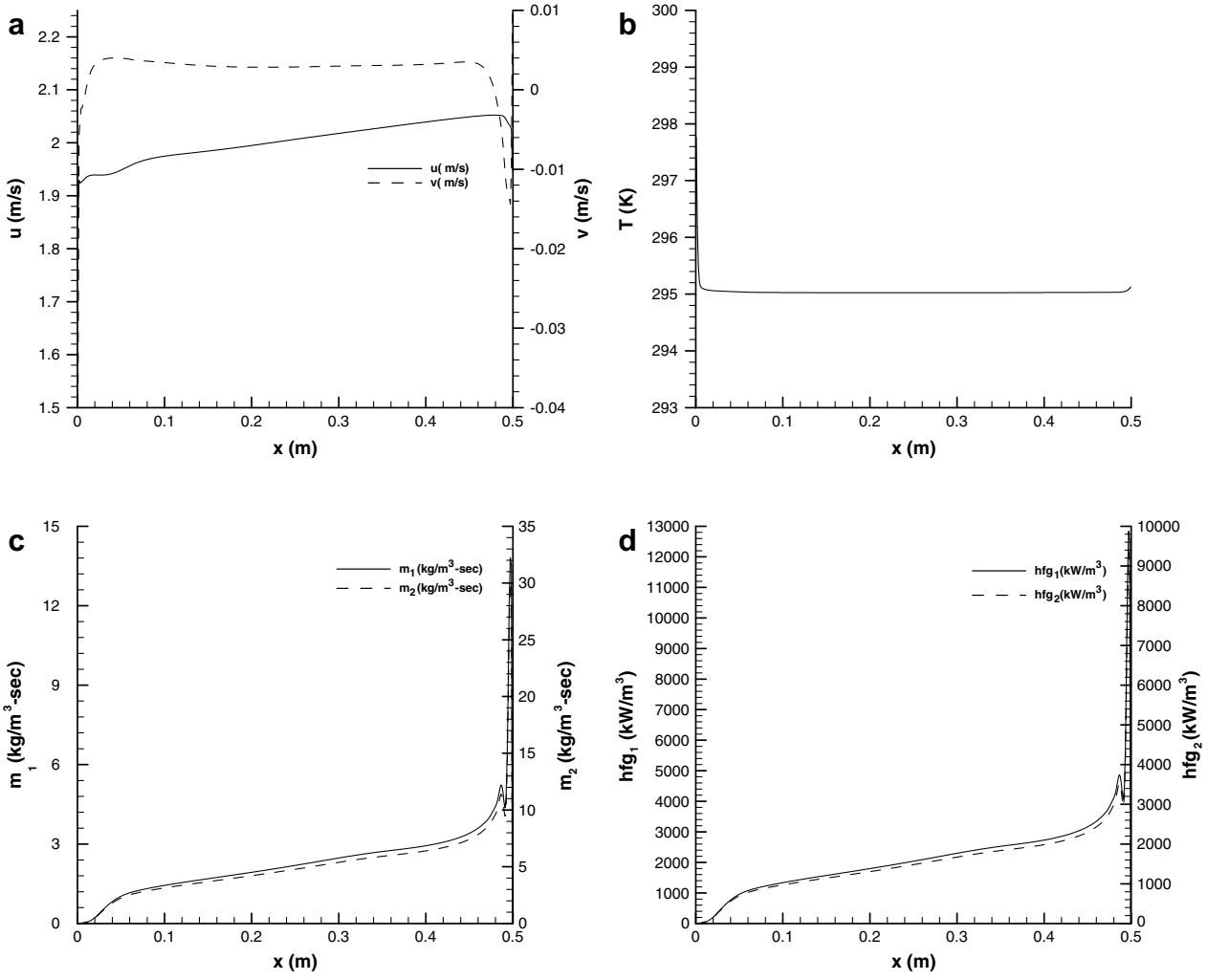

Fig. 7. (a) *x*- and *y*-velocity profiles; (b) temperature; (c) ethanol and *iso*-octane evaporation rate; (d) ethanol and *iso*-octane latent heat transfer at liquid/gas interface.

in this simulation set and also for other simulation sets, latent heat transfer and evaporation rate is higher at $x = 0.35$ m than at $x = 0.15$ m because interface vapour mass fraction gradient reduces as the gas flows upstream in the channel. When the temperature is raised from 310 to 340 K, there is a marginal increase of 1.5% in the total latent heat transfer at $x = 0.35$ m. However, at $x = 0.15$ m, there is a decrease of 2.2% in the total latent heat transfer. A similar change is also seen in the total interfacial mass transfer. This may be because at higher exit temperature, evaporation rate increases close to the channel exit, which in turn results in higher latent heat transfer. This causes a sharper drop in the interfacial temperature upstream results lower evaporation rates upstream. Indeed, it can be seen from the figure that interfacial temperature drop between the two location is largest when exit temperature is at 340 K and is almost negligible at 310 K. Interfacial liquid mass fraction of ethanol is slightly decreasing at both locations, however, the decrease is more prominent at $x = 0.15$ m. Interfacial vapour mass fraction increases with temperature for both ethanol and *iso*-octane.

When exit pressure is increased, it increases the velocity of the reverse flowing gas phase. As seen in Fig. 10, with increased exit pressure, there is a significant increase in the latent heat transfer and evaporation rate. When pressure is raised from 30 Pa (gauge) to 90 Pa (gauge), the increase in the latent heat transfer and evaporation rate is about 93% at $x = 0.15$ m and about 81% at $x = 035$ m. Mass fraction of liquid ethanol at the interface also rises with increase in exit pressure indicating higher mass transfer rate of *iso*-octane. However, rate of increase reduces with increase in pressure. Interfacial temperature at $x = 0.35$ m continuously decreases with increase in exit pressure. However, at $x = 0.15$ m, the temperature rises when pressure is increased from 30 Pa (gauge) to 50 Pa (gauge). After that the temperature decreases. It must be noted that interfacial heat transfer occurs due sensible and latent heat transfer. As the gas phase is entering the channel at a higher temperature than the liquid phase, sensible heat transfer takes place from the gas phase to the liquid phase. Sensible heat transfer is also strongly dependent on the composition of the fluids. At $x = 0.35$ m, due to higher evaporation rate, latent heat transfer predominates over sensible heating and therefore interfacial temperature is reducing with increasing exit pressure. However, at $x = 0.15$ m, evaporation rate is lower and therefore sensible heat transfer becomes important. When exit pressure is increased from 30 Pa (gauge) to 50 Pa (gauge), sensible heat transfer coupled with higher ethanol mass fraction in the liquid phase seem to results in increased interfacial temperature. However, at higher exit pressure, latent heat transfer starts predominating and therefore the temperature reduces. With increased evaporation rate, there is a steady rise of both ethanol and *iso*-octane vapour mass fraction at both locations.

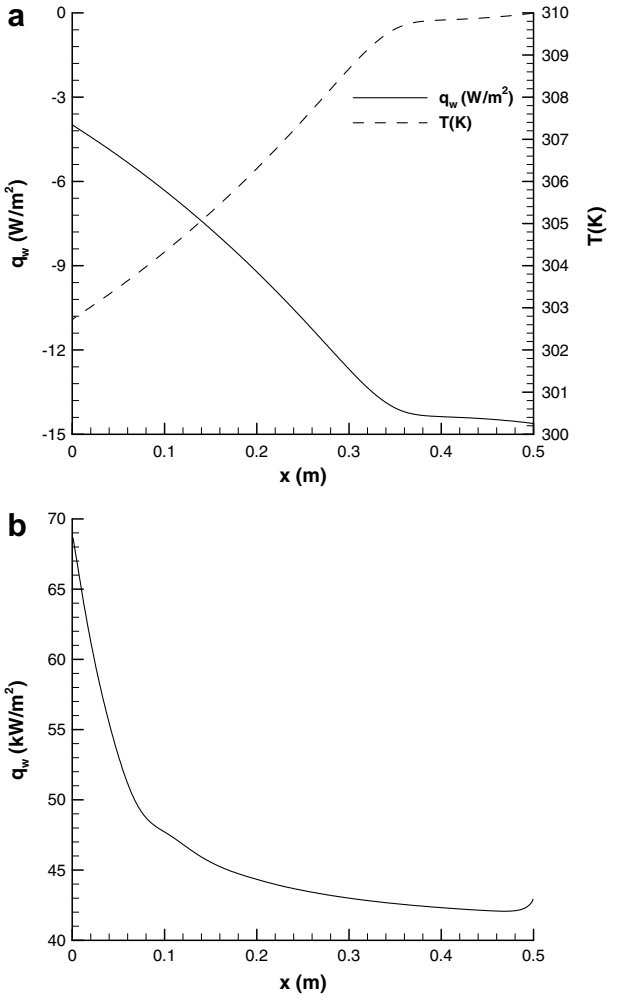

Fig. 8. (a) Heat flux and temperature profile at the top wall and (b) heat flux at the bottom wall.

In simulation Set 3, the composition of the air/vapour mixture entering the channel is changed. The results from this case is shown in Fig. 11. When the composition of the gas phase entering the channel is changed, gradient of the vapour at the interface changes, which in turn changes the evaporation rate of the liquid. Other than the base case, all the other cases in this set have 10% relative humidity of the either ethanol or *iso*-octane vapour or both. Relative humidity is defined as the ratio of vapour mole fraction to the saturation mole fraction of the pure fluid at a given temperature. As expected, latent heat transfer and evaporation rate is highest when relative humidity of both ethanol and *iso*-octane vapour is zero. When the air entering the channel has 10% *iso*-octane vapour, both latent heat transfer and evaporation rate decreases. This is because the evaporation rate of *iso*-octane is depressed, which also reduces its latent heat transfer contribution. The evaporation rate of ethanol remains almost unchanged. However, when there is 10% ethanol vapour, the total latent heat transfer decreases but evaporation rate increases. In this case, evaporation rate of ethanol is depressed and therefore its contribution to the total heat latent transfer is also reduced. The evaporation rate and latent heat transfer contribution of *iso*-octane is close to the base case. As the molecular weight of ethanol is lower than *iso*-octane, the decrease in total evaporation rate from the base case is less severe than the previous case. On the contrary, latent heat of vapourization of ethanol is higher than *iso*-octane and therefore the decrease in total latent heat transfer is more than the previous case. Total evaporation rate and latent heat transfer is minimum when the relative humidity of both ethanol and *iso*-octane is increased to 10%. The rise and fall of interfacial liquid ethanol mass fraction closely corresponds to the evaporation rates of the four cases. Similarly, interfacial temperature corresponds to the profile of latent heat transfer. It must be noted that the difference in the interfacial temperature at $x = 0.15$ and 0.35 m is highest when the relative humidity of ethanol and *iso*-octane vapour is 10%. It subsequently decreases when the relative humidity of both the components is reduced to zero. The change in vapour mass fraction corresponds to the liquid evaporation rate.

In simulation Set 4, liquid inlet temperature is changed. As can be seen from Fig. 12, interfacial heat and mass transfer is very strongly dependent on the inlet temperature. The increase in total evaporation rate and latent heat transfer when inlet temperature is increased from 295 to 340 K is more 550%. As can be seen from Eqs. (12)–(18), liquid–vapour equilibrium condition is determined from

vapour pressure at the interface, which in turn is directly dependent on liquid temperature. Similarly, as can be seen from the correlations given in Appendix, latent heat of evaporation is also dependent on vapour pressure. As in the previous simulations sets, evaporation rate and latent heat transfer is higher at $x = 0.35$ m than at $x = 0.15$ m. Interfacial ethanol mass fraction in the liquid phase increases with temperature, indicating that evaporation of *iso*-octane is increasing at a faster rate than ethanol. As expected,

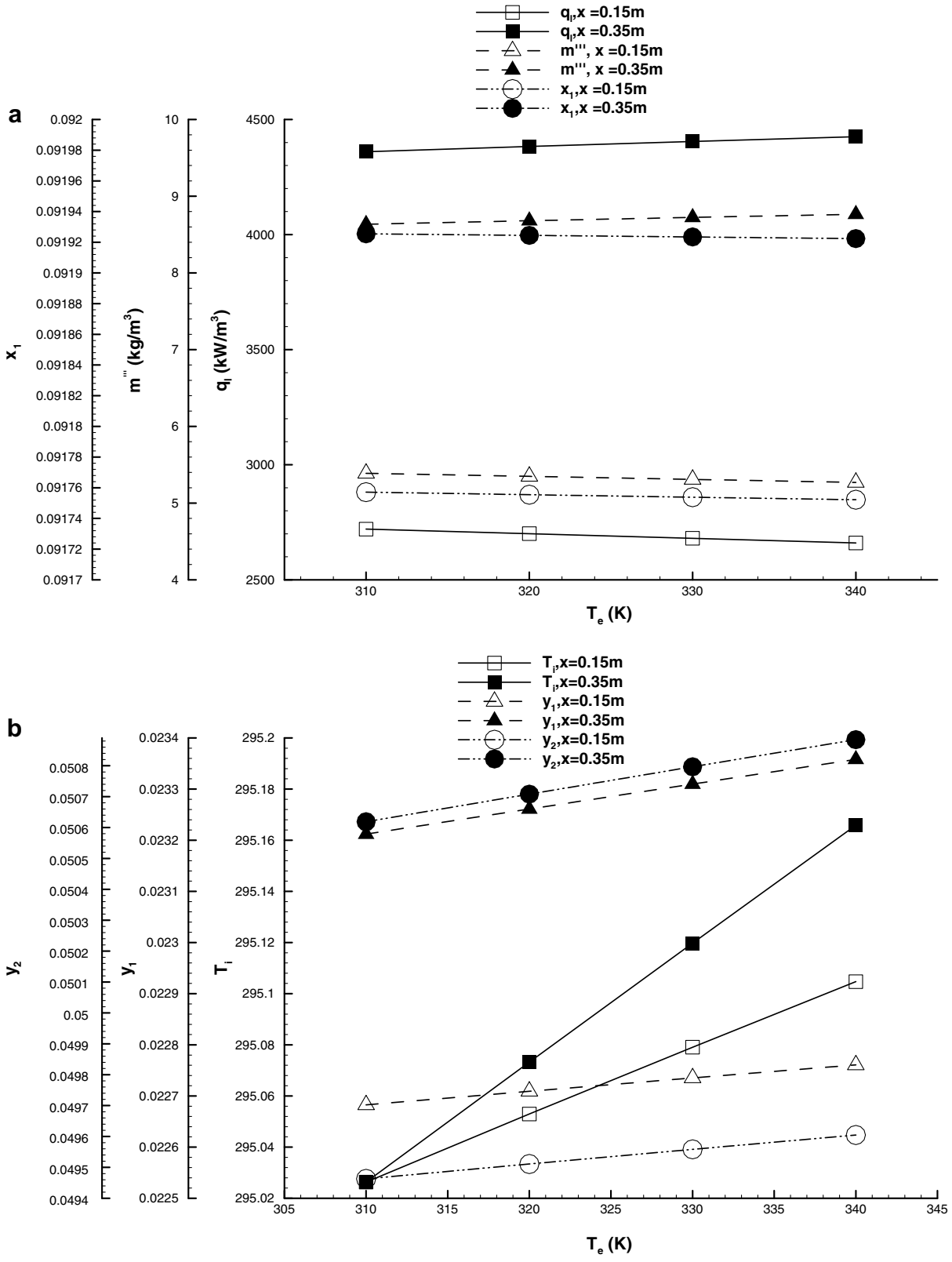

Fig. 9. Parameters at liquid/gas interface from simulation Set 1: (a) latent heat, evaporation rate, liquid ethanol mass fraction; (b) temperature, ethanol vapour mass fraction and *iso*-octane vapour mass fraction.

interfacial liquid temperature rises linearly with inlet temperature. Due increased interfacial mass transfer, mass fraction of ethanol and *iso*-octane in the gas phase also rises with temperature.

As shown in Fig. 2, vapour pressure of ethanol/*iso*-octane mixture is higher than the vapour pressure of its constituent components in pure form. This is because it is a non-ideal mixture. Hence, simulation Set 5 was performed to determine the effect of mixture composition on interfacial heat and mass transfer. Fig. 13 shows the results from this simulation set. Pure *iso*-octane has the lowest vapour pressure. When small amount of ethanol is introduced in *iso*-octane, there is significant rise in vapour pressure. It reaches the peak value of vapour pressure when the mole fraction of ethanol is 0.2. It remains close to this peak value till mole fraction of ethanol is approximately 0.8. Further increase in ethanol composition in the mixture results is a decrease in vapour pressure. This trend is closely followed by the latent heat and

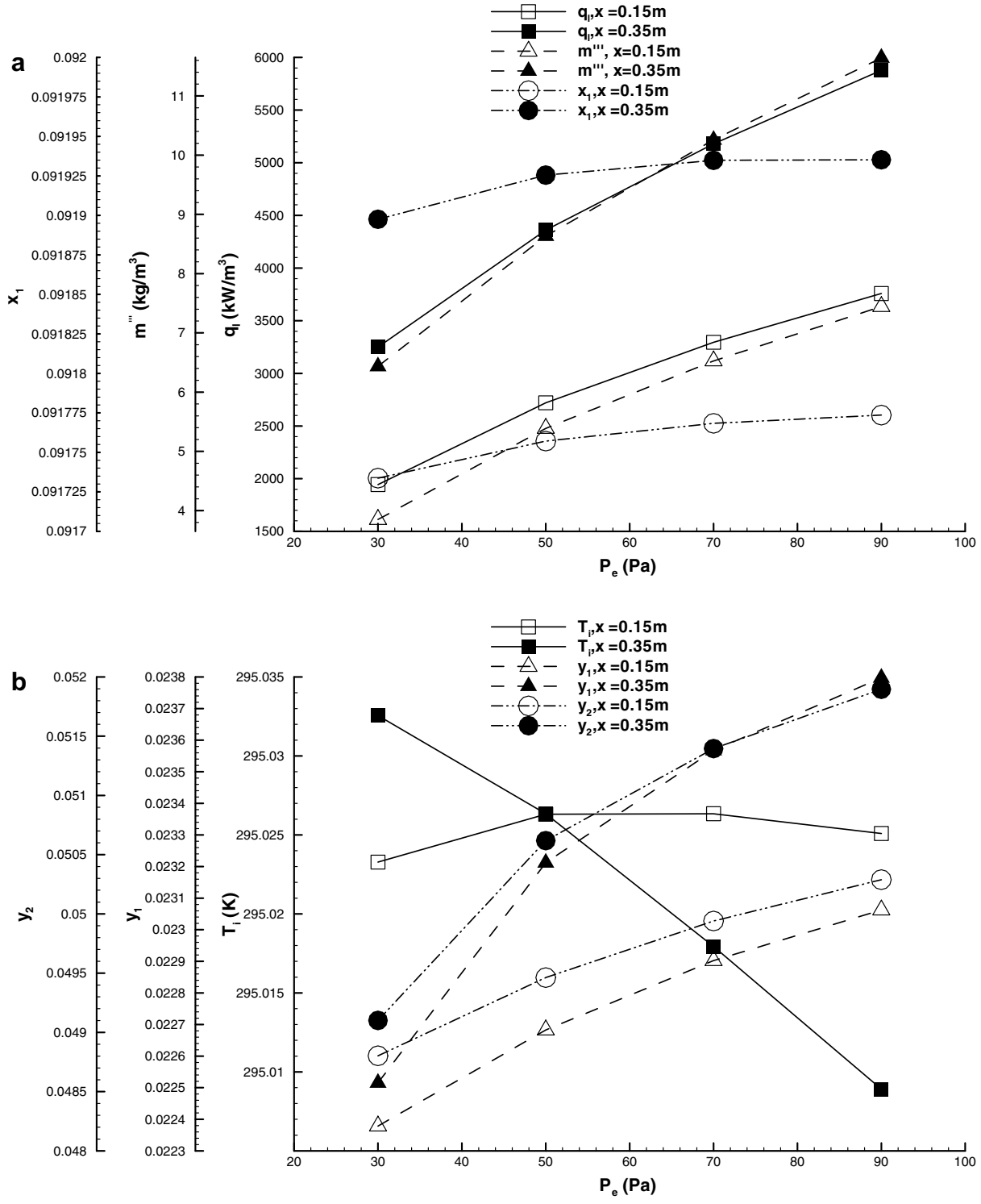

Fig. 10. Parameters at liquid/gas interface from simulation Set 2: (a) latent heat, evaporation rate, liquid ethanol mass fraction; (b) temperature, ethanol vapour mass fraction and *iso*-octane vapour mass fraction.

interfacial mass transfer rate plots. Latent heat transfer is least for pure *iso*-octane. It is marginally higher for pure ethanol. The total latent heat transfer is significantly higher for intermediate values of ethanol composition, though there is slight decrease in value as the mole fraction of liquid ethanol is increased from 0.2 to 0.8. Evaporation rate is lowest for pure ethanol and it is marginally higher for pure *iso*-octane. Evaporation rate increases when liquid mole fraction of ethanol is 0.2. At $x = 0.15$ m, the evaporation rate

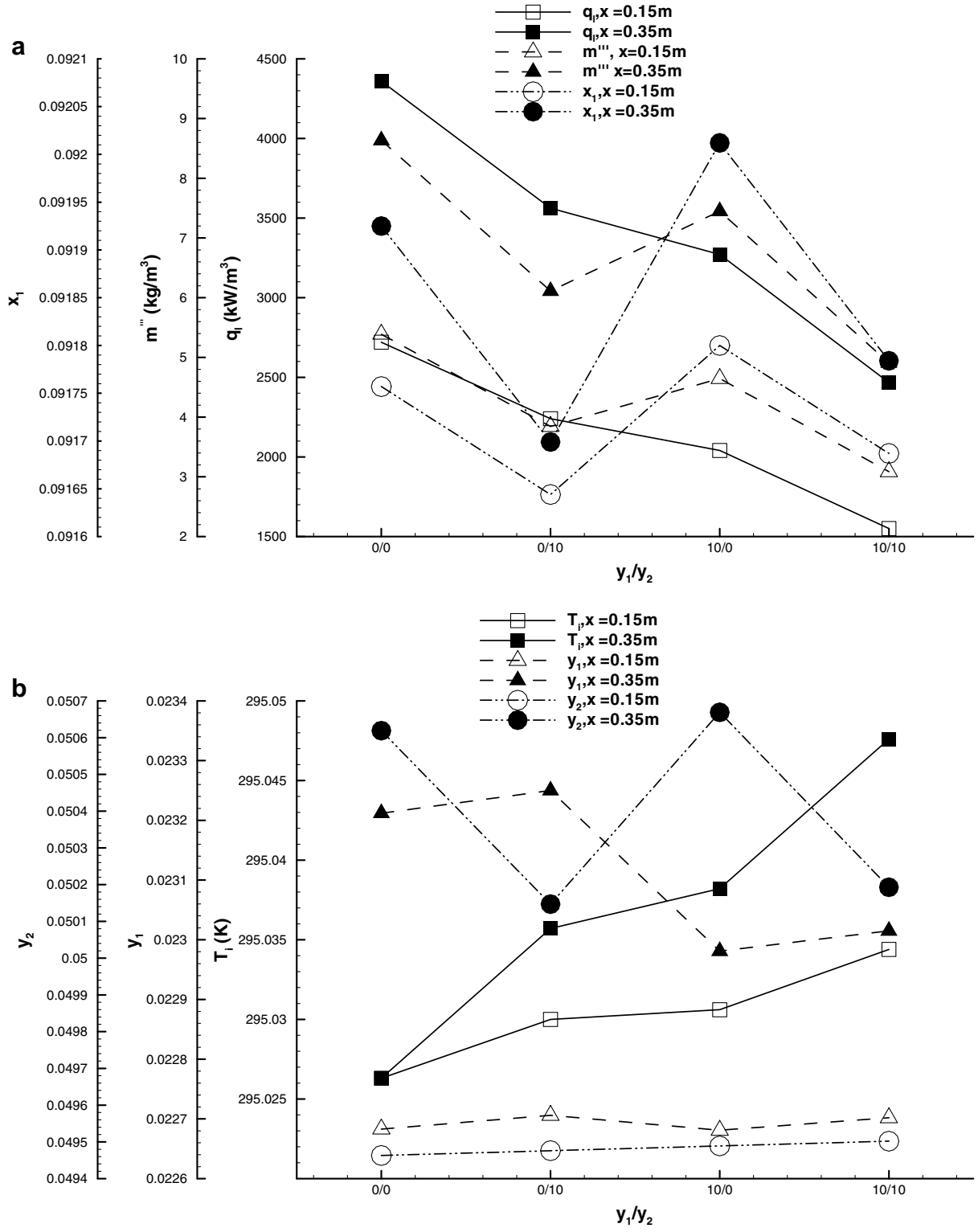

Fig. 11. Parameters at liquid/gas interface from simulation Set 3: (a) latent heat, evaporation rate, liquid ethanol mass fraction; (b) temperature, ethanol vapour mass fraction and *iso*-octane vapour mass fraction.

reduces slightly when liquid ethanol mole fraction is increased from 0.2 to 0.8. However, at $x = 0.35$ m, there is slight increase in the evaporation rate when ethanol mole fraction is increased from 0.2 to 0.5, but it then reduces when it is further raised to 0.8. Interfacial temperature at $x = 0.35$ m is higher than at $x = 0.15$ m for pure *iso*-octane. This indicates that even though evaporation rate is higher at $x = 0.35$ m, sensible heat predominates over latent heat transfer. This is because; latent of heat of vapourization of pure *iso*-octane is less. When mole fraction of ethanol is increased to 0.2, interfacial temperature at the two locations is almost same. When it is further increased to 0.5 and 0.8, the interface temperature is lower at $x = 0.35$ m and the temperature differential between the locations increases with increasing ethanol content. Reason for this can be explained using the values given in Table 3. Thermal diffusion at the liquid surface is directly proportional to interfacial turbulence intensity and inversely proportional to the product of density and specific heat. As can be seen from the table, both turbulence intensity and the product of density and specific heat increases with ethanol content. However, the rate of increase in the product of density and specific heat is higher than turbulence

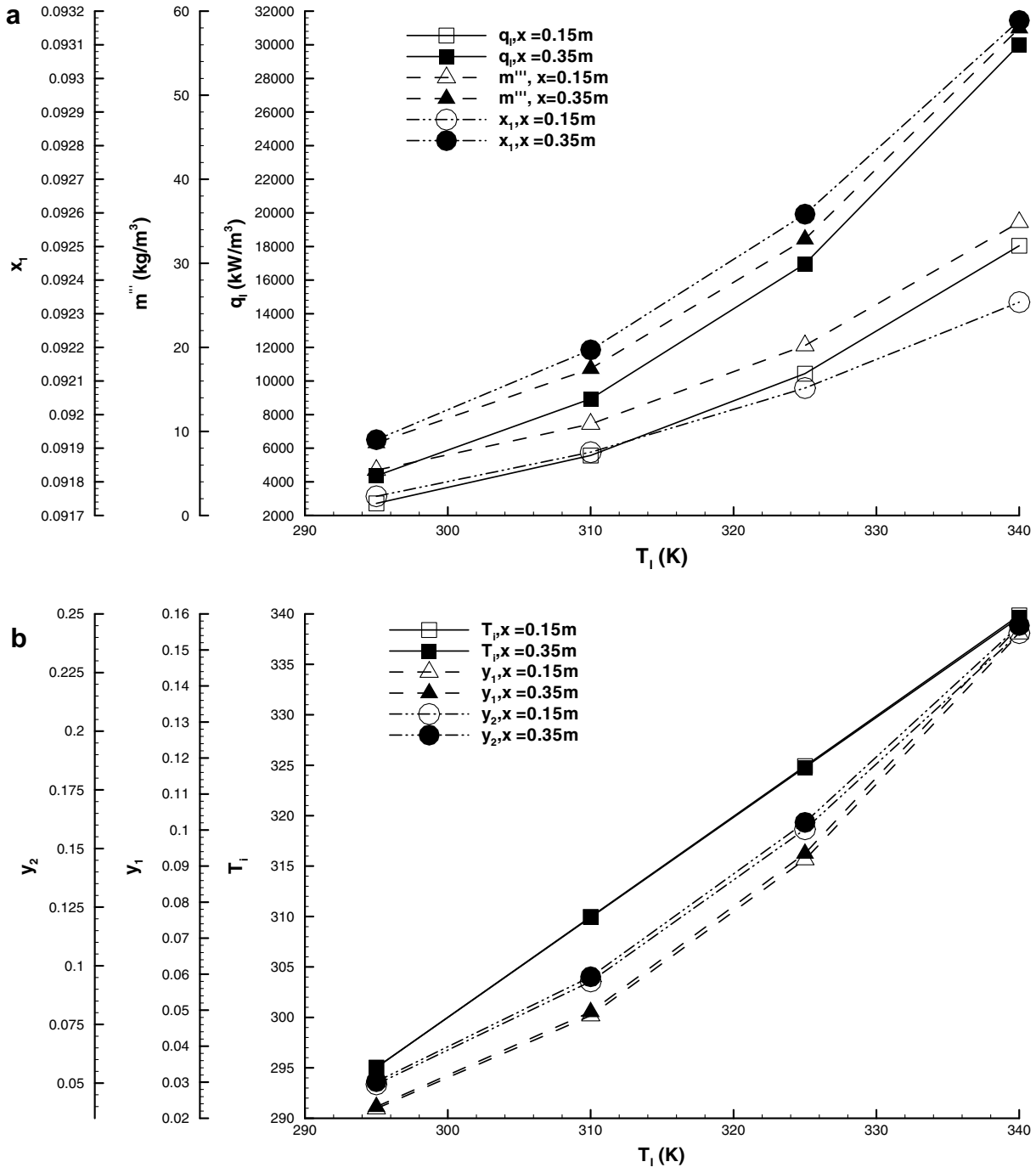

Fig. 12. Parameters at liquid/gas interface from simulation Set 4: (a) latent heat, evaporation rate, liquid ethanol mass fraction; (b) temperature, ethanol vapour mass fraction and *iso*-octane vapour mass fraction.

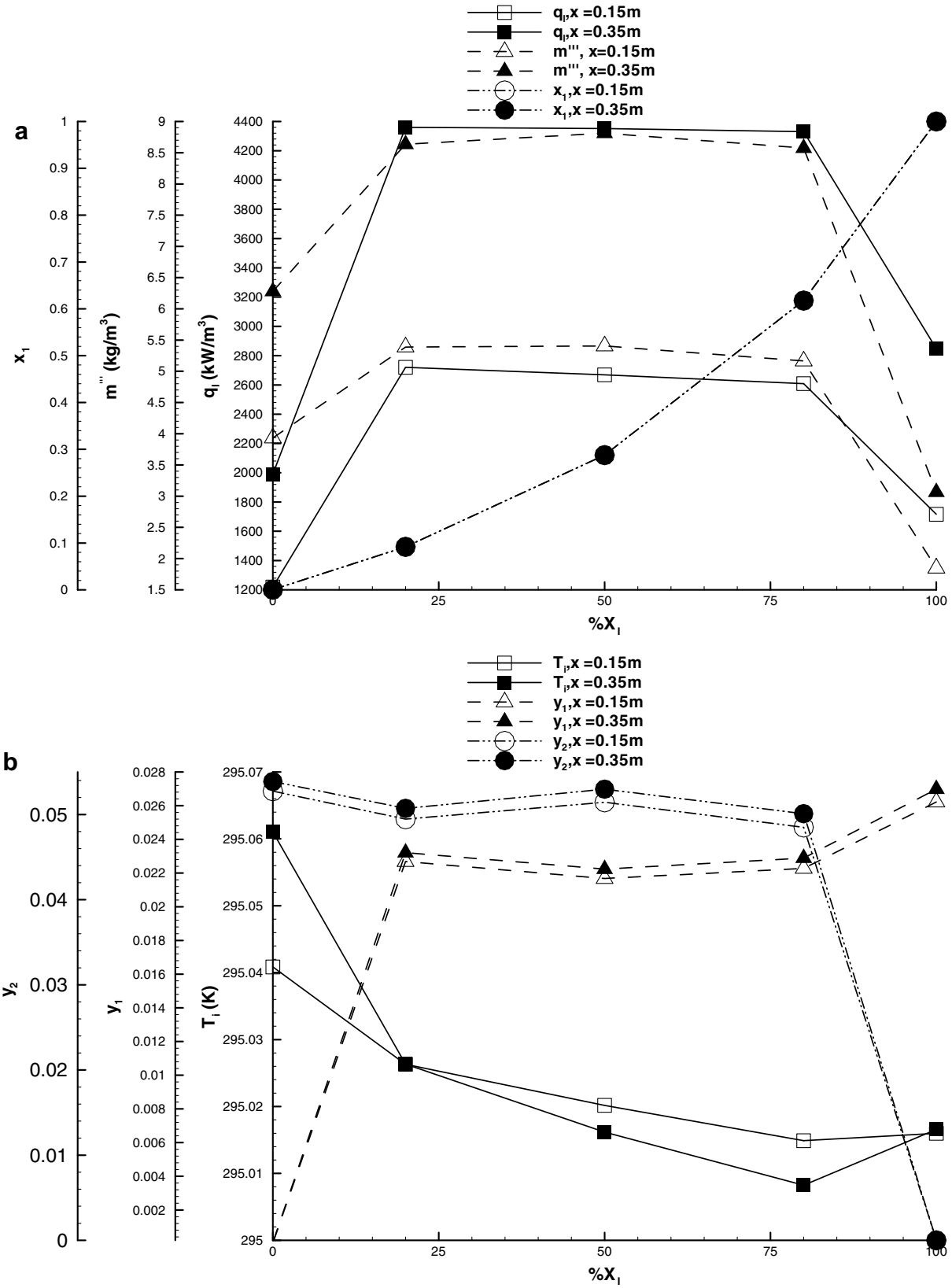

Fig. 13. Parameters at liquid/gas interface from simulation Set 5: (a) latent heat, evaporation rate, liquid ethanol mass fraction; (b) temperature, ethanol vapour mass fraction and *iso*-octane vapour mass fraction.

intensity. Therefore, even though latent heat transfer is almost same, interfacial temperature decreases when ethanol mole fraction is increased from 0.2 to 0.8. It again increases for pure ethanol as latent heat transfer decreases.

Table 3
Turbulence intensity and product of liquid density and specific heat from simulation Set 5

Liquid ethanol mole fraction	x = 0.15 m		x = 0.35 m	
	%I	ρC_p (kJ/m^3 K)	%I	ρC_p (kJ/m^3 K)
0.0	43.62	1416.99	44.35	1417.25
0.2	43.29	1493.25	44.10	1493.38
0.5	43.34	1630.41	44.54	1630.54
0.8	43.52	1819.38	45.19	1819.51
1.0	44.54	2008.11	46.82	2008.11

5. Conclusion

In this study an evaporation model for a binary mixture of ethanol and *iso*-octane was developed in conjunction with VOF multiphase model. This model was used to study the effect of liquid inlet temperature and composition, exit pressure, temperature and gas composition in counter-current stratified two-phase flow system. Based on the parametric study, some of the general conclusions are:

- In counter-current flow system, interfacial heat and mass transfer is higher near the channel exit and it gradually decreases from the exit to the inlet of the channel.
- Even though ethanol has a higher vapour pressure than *iso*-octane, the molecular weight of *iso*-octane is higher than ethanol and therefore, its evaporation rate in term of mass per unit time is higher. Hence, mass fraction of liquid ethanol near the liquid/gas interface increases along the length of the channel.
- Among the various parameters varied, liquid inlet temperature has the most profound effect on interfacial heat and mass transfer. Total evaporation rate and latent heat transfer increases by more that 550% when liquid inlet temperature is raised from 295 to 340 K.
- Due to the non-ideal nature of the mixture, interfacial heat and mass transfer of ethanol/*iso*-octane mixture is significantly higher than its constituents in pure form.

It was found that when bottom wall temperature and top wall heat transfer coefficient were changed, there was no significant change in the interfacial heat and mass transfer. Therefore, those results were not reported this study. Though this study was performed for a 2D-channel flow, this algorithm is very flexible and can therefore be used to study practical systems of complex geometries and highly turbulent flows.

Appendix

VLE and thermophysical properties in the liquid and gas phase were calculated using the following relations [34]:

- Vapour pressure
  - *Ethanol*

  Wagner method was used to calculate vapour pressure for ethanol

$$\ln\left(\frac{P_{\text{vap}}}{P_{\text{C}}}\right)=\frac{a\tau+b\tau^{1.5}+c\tau^{2.5}+d\tau^{5}}{1-\tau}$$

where,

$$a=-8.68587;\quad b=1.17831;\quad c=-4.8762;\quad d=1.5880;$$
$$\tau=1-T/T_{\text{C}}$$

  - *iso-Octane*

  Antoine method was used to calculate vapour pressure for *iso*-octane

$$\log_{10}(P_{\text{vap}})=A-\frac{B}{T+C-273.15}$$

where,

$$A=3.93646;\quad B=1257.85;\quad C=220.767$$

- Latent heat of vapourization

$$-\frac{\mathrm{d}(\ln P_{\text{vap}}/P_{\text{C}})}{\mathrm{d}(1/T_{\text{r}})}=\frac{h_{\text{fg}}}{RT_{\text{C}}\Delta Z_{\text{V}}}=\psi$$

where

$$\Delta Z_{\text{V}}=Z_{\text{g}}-Z_{\text{l}}$$

ψ is calculated from the vapour pressure equation. Therefore,
  - *Ethanol*

  As Wagner method was used to determine vapour pressure, therefore,

$$\psi=-a+b\tau^{0.5}(0.5\tau-1.5)+c\tau^{1.5}(1.5\tau-2.5)+d\tau^{4}(4\tau-5)$$

  - *iso-Octane*

  As Antoine method was used to determine vapour pressure, therefore,

$$\psi=\frac{2.303}{T_{\text{C}}}B\left[\frac{T_{\text{r}}}{T_{\text{r}}+\left(\frac{C-273.15}{T_{\text{C}}}\right)}\right]^{2}\quad\text{and}\quad T_{\text{r}}=\frac{T}{T_{\text{C}}}$$

Compressibility factor Z is calculated from Peng and Robinson equation of state.

- Binary diffusivity

  Fuller method was used to determine diffusivity in the gas phase

$$D_{ij}=\frac{0.0143T^{1.75}}{PM_{ij}^{1/2}\left[\left(\sum_{V}^{i}\right)^{1/3}+\left(\sum_{V}^{j}\right)^{1/3}\right]^{2}}$$

where,

$$\frac{2}{M_{ij}}=\frac{1}{M^{i}}+\frac{1}{M^{j}}$$

and $\sum_V$ is found for each component by summing atomic diffusion volumes given in Ref. [34]. For ethanol, *iso*-octane and air, the respective values are 51.77, 168.78 and 19.7.

- Gas phase mixture properties
  - *Density*

  Gas phase density is calculated from partial pressure of individual components in the mixtures by using Dalton's law

$$\rho=\sum_{i=1}^{N}\rho^{i}$$

where,

$$\rho^{i}=\frac{x^{i}PM^{i}}{Z^{i}RT}$$

Compressibility factor Z_i for vapour is determined from Peng and Robinson equation for state. In the above calculation, ambient pressure and local temperature have been used. Z_i was assumed to be unity for air.
  - *Viscosity*

Wilke method has been used to determine the vapour viscosity. It is expressed as

$$\mu^{\text{m}}=\sum_{i=1}^{N}\frac{x^{i}\mu^{i}}{\sum_{j=1}^{N}x^{j}\varphi_{ij}}$$

where

$$\varphi_{ij} = \frac{[1 + (\mu^i/\mu^j)^{1/2}(M^j/M^i)^{1/4}]^2}{[8(1 + M^i/M^j)]^{1/2}}$$

◦ *Thermal conductivity*

Thermal conductivity of air–vapour mixture is determined as above. However, an additional factor proposed by Mason and Saxena was used

$$k^{\mathrm{m}} = \sum_{i=1}^{N} \frac{x^i k^i}{\sum_{j=1}^{N} x^j A_{ij}}$$

where

$$A_{ij} = \frac{\varepsilon[1 + (k^i/k^j)^{1/2}(M^j/M^i)^{1/4}]^2}{[8(1 + M^i/M^j)]^{1/2}}, \quad \varepsilon = 1.065$$

◦ *Effective diffusivity*

It is defined as

$$D^i_{\mathrm{eff}} = \rho D^{i,\mathrm{m}} + \frac{\mu_t}{Sc_t}$$

where

$$D^{i,\mathrm{m}} = \frac{1 - x^i}{\sum_{j,j\neq i} x^j/D_{ij}}$$

and D_{ij} is calculated from Fuller method as explained above.

- Liquid phase mixture properties
  - ◦ *Density*

  Liquid density is calculated from volumetric composition

$$\rho = \sum_{i=1}^{N} X^i \rho^i$$

◦ *Viscosity*

It calculated using Grunberg and Nissan method

$$\ln(\mu^{\mathrm{m}}) = \sum_{i}^{N} X^i \ln(\mu^i)$$

◦ *Thermal conductivity*

It is calculated using Power Law method

$$k^{\mathrm{m}} = \left[\sum_{i=1}^{N} Y^i (k^i)^{-2}\right]^{-1/2}$$

◦ *Specific heat*

$$C_p^{\mathrm{m}} = \sum_{i=1}^{N} Y^i C_p^i$$

References

[1] J. Schroppel, F. Thiele, On the calculation of momentum, heat and mass transfer in laminar and turbulence boundary layer along a vaporizing liquid film, Numer. Heat Transfer 6 (4) (1983) 475–496.

[2] Siu-Ming Yih, Jung-Liang Liu, Prediction of heat transfer in turbulent falling liquid films with or without interfacial shear, AIChE J. 29 (6) (1983) 903–909.

[3] T.R. Shembharkar, B.R. Pai, Prediction of film cooling with a liquid coolant, Int. J. Heat Mass Transfer 29 (6) (1986) 899–908.

[4] Y.L. Tsay, T.F. Lin, Combined heat and mass transfer in laminar gas stream flowing over an evaporating liquid film, Wärme-und Stoffübertrangung 25 (4) (1990) 221–231.

[5] M. Feddaoui, A. Mir, E. Belahmidi, Concurrent turbulent mixed convection heat and mass transfer in falling film of water inside a vertical heated tube, Int. J. Heat Mass Transfer 46 (18) (2003) 3497–3509.

[6] Jer-Huan Jang, Wei-Mon Yan, Thermal protection with liquid film in turbulent mixed convection channel flows, Int. J. Heat Mass Transfer 49 (19–20) (2006) 3645–3654.

[7] Ross Taylor, Coupled heat and mass transfer in multicomponent systems: solution of the Maxwell–Stefan equations, Lett. Heat Mass Transfer 8 (5) (1981) 405–416.

[8] R. Carty, T. Schrodt, Concentration profiles in ternary gaseous diffusion, Ind. Eng. Chem. Fundam. 14 (3) (1975) 276–278.

[9] Vijay R. Mhetar, John C. Slattery, The Stephan problem of a binary liquid mixture, Chem. Eng. Sci. 52 (8) (1997) 1237–1242.

[10] Constantine M. Megaridis, Liquid-phase variable property effects in multicomponent droplet convective evaporation, Combust. Sci. Technol. 92 (4–6) (1993) 291–311.

[11] R. Kneer, M. Schneider, B. Noll, S. Wittig, Diffusion controlled evaporation of a multicomponent droplet: theoretical studies on the importance of variable liquid properties, Int. J. Heat Mass Transfer 36 (9) (1993) 2403–2415.

[12] M. Renksizbulut, M. Bussmann, Multicomponent droplet evaporation at intermediate Reynolds numbers, Int. J. Heat Mass Transfer 36 (11) (1993) 2827–2835.

[13] P.L.C. Lage, R.H. Rangel, C.M. Hackenberg, Multicomponent heat and mass transfer for flow over a droplet, Int. J. Heat Mass Transfer 36 (14) (1993) 3573–3581.

[14] P. Bhattacharya, S. Ghosal, S.K. Som, Evaporation of multicomponent liquid fuel droplets, Int. J. Energy Res. 20 (5) (1996) 385–398.

[15] M. Burger, R. Schmehl, K. Prommersberger, O. Schäfer, R. Koch, S. Wittig, Int. J. Heat Mass Transfer 46 (23) (2003) 4403–4412.

[16] Cláudio P Ribeiro Jr., Cristiano P. Borges, Paulo L.C. Lage, Modelling of direct-contact evaporation using simultaneous heat and multicomponent mass-transfer model for superheated bubbles, Chem. Eng. Sci. 60 (6) (2005) 1761–1772.

[17] Y. Taitel, A. Tamir, E.U. Schlünder, Evaporation of liquid mixtures in laminar flow, Chem. Eng. J. 8 (3) (1974) 227–234.

[18] E. Ya. Kenig, L.P. Kholpanov, Simultaneous mass and heat transfer with reactions in a multicomponent laminar falling liquid film, Chem. Eng. J. 49 (2) (1992) 119–126.

[19] J.W. Palen, Qi. Wang, J.C. Chen, Falling film evaporation of binary mixtures, AIChE J. 40 (2) (1994) 207–214.

[20] M. Braun, Renz, Multicomponent diffusion interactions during condensation in laminar and turbulent flow, Int. J. Heat Mass Transfer 40 (1) (1997) 131–139.

[21] W.W. Baumann, F. Thiele, Heat and mass transfer in evaporating two-component liquid film flow, Int. J. Heat Mass Transfer 33 (2) (1990) 267–273.

[22] M. Gerendas, S. Wittig, Experimental and numerical investigation on evaporation of shear-driven multicomponent liquid wall films, ASME J. Eng. Gas Turb. Power 123 (3) (2001) 580–588.

[23] W.M. Yan, T.F. Lin, Combined heat and mass transfer in natural convection between vertical parallel plates with film evaporation, Int. J. Heat Mass Transfer 33 (3) (1990) 529–541.

[24] C.W. Hirt, B.D. Nichols, Volume of fluid (VOF) method for the dynamics of free boundaries, J. Comput. Phys. 39 (1) (1981) 201–225.

[25] Damir Juric, Grétar Tryggvason, Computations of boiling flows, Int. J. Multiphase Flow 24 (3) (1998) 387–410.

[26] Ronald P. Fedkiw, Tariq Aslam, Barry Merriman, Stanley Osher, A non-oscillatory Eulerian approach to interfaces in multimaterial flows (the Ghost Fluid method), J. Comput. Phys. 152 (2) (1999) 457–492.

[27] M.G. Wohak, H. Beer, Numerical simulation of direct-contact evaporation of a drop rising in a hot, less volatile immiscible liquid of higher density – possibilities and limits of the SOLA-VOF/CSF algorithm, Numer. Heat Transfer Pt. A 33 (6) (1998) 561–582.

[28] Dalton J.E. Harvie, David F. Fletcher, A hydrodynamic and thermodynamic simulation of droplet impacts on hot surfaces. Part I: Theoretical model, Int. J. Heat Mass Transfer 44 (14) (2001) 2633–2642.

[29] Malcolm R. Davidson, Murray Rudman, Volume-of-Fluid calculation of heat or mass transfer across deforming interfaces in two-fluid flow, Numerical Heat Transfer, Part B 41 (3&4) (2002) 291–308.

[30] Samuel W.J. Welch, Thami Rachidi, Numerical computation of film boiling including conjugate heat transfer, Numer. Heat Transfer Pt. B 42 (1) (2002) 35–53.

[31] D.K. Agarwal, S.W.J. Welch, G. Biswas, F. Durst, Planar simulation of bubble growth in film boiling in near-critical water using a variant of the VOF method, ASME J. Heat Transfer 126 (3) (2004) 329–338.

[32] FLUENT User Manual, version 6.3, Fluent Inc., Lebanon, NH, USA.

[33] R. Banerjee, K.M. Isaac, Evaluation of turbulence closure schemes for stratified two-phase flow, in: 2003 ASME International Mechanical Engineering Congress and Exposition, Washington, DC, 2003.

[34] B.E. Poling, J.M. Prausnitz, J.P. O'Connell, The Properties of Gases & Liquids, fifth ed., McGraw-Hill, New York, 2000.

[35] Dalton J.E. Harvie, David F. Fletcher, A simple kinetic theory treatment of volatile liquid–gas interfaces, ASME J. Heat Transfer 123 (3) (2001) 486–491.

[36] R. Banerjee, K.M. Isaac, An algorithm to determine mass transfer rate from a pure liquid surface using VOF multiphase model, Int. J. Engine Res. 5 (1) (2004) 23–37.

[37] R. Banerjee, A numerical study of combined heat and mass transfer in an inclined channel using VOF multiphase model, Numer. Heat Transfer Pt. A 52 (2) (2007) 163–183.

[38] S.V. Patankar, Numerical Heat Transfer and Fluid Flow, Taylor and Francis, Philadelphia, 1980.